

Ab initio calculations on some transition metal heptoxides by using effective core potentials

Ana M. Amado, Paulo J.A. Ribeiro-Claro*

Unidade Química-Física Molecular, Departamento de Química, Faculdade de Ciências e Tecnologia, Universidade de Coimbra, P-3049 Coimbra, Portugal

Received 14 August 1998; received in revised form 3 November 1998; accepted 26 November 1998

Abstract

The ab initio molecular structures and vibrational frequencies for several transition metal heptoxides $X_2O_7^{n-}$ ($n = 0, 2, 4$) were calculated using effective core potentials at the HF and DFT (B3LYP) levels. The relative merits of different valence basis set arrangements were tested by comparison with experimental results available, in particular with gas-phase Re_2O_7 molecular structure and vibrational frequencies. The calculations were then extended to other heptoxides of the VB, VIB and VIIB transition metal groups. The results indicate that a staggered geometry (either D_{3d} or C_2) is the energy minimum for most of the heptoxides studied. The only exceptions are Mn_2O_7 , which clearly prefers an eclipsed $C_{2v(syn)}$ configuration, and Tc_2O_7 , for which C_2 and $C_{2v(syn)}$ geometries have nearly the same energy.

Particular attention was given to the magnitude of the X–O–X bond angle, as this structural parameter has been a matter of some controversy. The calculated values range from 125° (Mn_2O_7) to 180° (Group VB heptoxides) and depend on the position of the transition metal in the Periodic Table. A tendency for linearity of the X–O–X moiety on going both downwards the group and backwards the period was observed and discussed. © 1999 Elsevier Science B.V. All rights reserved.

Keywords: Transition metal; Heptoxide; Molecular structures; Vibrational frequencies; Correlation energy; ab initio Calculations; Effective Core Potentials; B3LYP method

1. Introduction

In the last few years, the question of the linearity of the X–O–X moiety in different $X_2O_7^{n-}$ species has raised some attention. Several experimental techniques, ranging from X-ray and electron diffraction to vibrational and NMR spectroscopy were used in order to get some insights on this structural feature. However, contradictory results are often reported.

For instance, while an initial electron diffraction

study on Re_2O_7 , revealed a nearly linear Re–O–Re bond angle [1], a reinvestigation by Kiprof et al. [2] has shown a bent arrangement of that moiety, confirmed recently by gas-phase vibrational spectroscopy [3]. For ditechneum heptoxide, Tc_2O_7 , X-ray studies point to an exactly linear configuration around the central O-atom [4,5], but a recent vibrational spectroscopic study in the gas-phase suggests a non-linear structure [3], similar to that found for Re_2O_7 .

Some of the reported discrepancies arise from the well-known crystal structure dependence on the radii and on the polarizing properties of the counter-ion in the crystal. In fact, a great variety of X–O–X bond angles were determined by X-ray for the same $X_2O_7^{n-}$

* Corresponding author. Tel.: + 351-39-26541; fax: + 351-39-26541.

E-mail address: claro@gemini.ci.uc.pt (P.J.A. Ribeiro-Claro)

unit with different cations [6]. For example, while in $K_2Mo_2O_7 \cdot KBr$ the Mo–O–Mo linkage is linear [7], the $Mo_2O_7^{2-}$ ion in $MgMo_2O_7$ shows a bridge bond angle of 160.7° [8]. In a recent publication, Griffith et al. [9] concluded that the Mo–O–Mo linkage in $Mo_2O_7^{2-}$ hydrogen-bonded to binaphthol units is bent and that the initially suggested linear structure results from a significant thermal anisotropy exhibited by the bridging oxygen atom.

Quantum chemical methods, in particular ab initio calculations, are nowadays very powerful tools in chemical research, although limited by the huge computational costs associated with the large number of electrons in systems such as transition metal compounds. The development of effective core potentials (ECPs) has to some extent overcome this limitation. In fact, by replacing the inert core electrons by a fixed potential, this approach substantially reduces the computational effort, as the SCF calculations are restricted to the valence electrons. In addition, the relativistic effects can be easily included in the ECPs, turning the ab initio calculations on transition metal containing compounds both feasible and accurate [10].

In addition, the electron correlation effects appear to be treated accurately with the new generation of “gradient-corrected” density functional theories (DFT) [10]. In fact, the number of applications of this computational combination (ECP/DFT) to inorganic complexes, particularly to transition metal compounds, is increasing rapidly and shows a good agreement with experiment with little additional computational demands [11–17].

In a previous publication [18], ab initio calculations at the HF level for several Vanadium (V) species using the ECP approach were reported. The relative merits of several published ECPs have been verified by comparison with published experimental data and with all-electron results also presented therein [18]. While a satisfactory general agreement was found between the theoretical and the published experimental results, a question remained on what concerns the V–O–V angle in the $V_2O_7^{4-}$ anion. In fact, while both all-electron and ECP results yielded a centrosymmetrical linear molecular structure (V–O–V = 180°), the published X-ray results refer to a preference for the bent geometry, although some linear species have been found [6] (see also footnote of Table 8 of Ref. [18]).

In this work, the structural preferences of several $X_2O_7^{n-}$ ($n = 0, 2, 4$) heptoxides, with special emphasis given to the magnitude of the X–O–X bond angle, are studied by ab initio calculations using the ECP approach at both HF and DFT levels. The work proceeded in two steps. First, the quality/computational cost ratio of different basis set arrangements were evaluated by comparison with experimental gas-phase data of the literature, in particular for Re_2O_7 . Then, the calculations were extended to other transition metal heptoxides of the VB (including vanadium), VIB and VIIB groups, using the selected ECP/basis set combination.

2. Computational methods

The calculations were performed using the Gaussian 94w program package [19] adapted to a Pentium II 300 MHz computer.

The ECPs used are those of Stevens et al. [20], for the oxygen atoms, and of Hay and Wadt [21], for the transition metal atoms (VB, VIB and VIIB periodic table groups). This combination (referred to as HS in our previous work on Vanadium (V) oligomeric species) has proved to be a good choice for this kind of systems [18].

The accuracy of the following basis set arrangement has been tested. On the oxygen atoms, both minimal (4/4) and double-zeta (31/31) splitting schemes have been tested. The effect of a polarization d ($\zeta = 0.8$) [22] and/or a diffuse sp ($\zeta = 0.0845$) [23] functions on both types of oxygen atoms (bridge and terminal, hereafter named as O_b and O_t , respectively) were verified.

For the transition metals, the small-core ECPs by Hay and Wadt [21], which are relativistic for the second- and third-row transition metals, have been used. Both minimal and double-zeta splittings ((55/5/ N) and (441/41/($N - 1$))1), with $N = 5, 4$ or 3 for the three rows, respectively) were tested. The larger core ECPs, developed by the same authors [24], have not been considered, as they were found inadequate for this kind of systems previously [10] and for other transition metal compounds [10,25–27].

In order to account for the electron correlation effects, the widely used hybrid method denoted by B3LYP [11,15–17,28,29], which includes a mixture

of HF and DFT exchange terms and the gradient-corrected correlation functional of Lee, et al. [30], as proposed and parametrized by Becke [31], has been considered.

For each studied heptoxide several possible configurations were used as starting points, and fully optimized. The order of the critical points ($\lambda = 0$ for minima, $\lambda = 1, 2, \dots$ for first and higher order saddle points) were evaluated at the HF level by computing the vibrational frequencies using numeric derivatives.

3. Results

3.1. Basis sets selection

As stated earlier, the first aim was the selection of a basis set combination that yields the best compromise between accuracy and computational costs on describing the experimental data available (in particular, the molecular structure and vibrational frequencies of gas phase Re_2O_7).

In this context, it was firstly concluded that the use of a minimal basis set at both oxygen and transition metal atoms, *was inadequate to describe the bent geometry of the X–O–X moiety reported for both gas phase Re_2O_7 and crystalline $\text{Cr}_2\text{O}_7^{2-}$, $\text{Mo}_2\text{O}_7^{2-}$ and Mn_2O_7 geometries.* Neither the splitting of the oxygen and/or transition metal basis sets nor the inclusion of a diffuse function on the O_t and/or O_b valence shells overcame this limitation.

The addition of a polarization function at the oxygen atoms, however, was found to be fundamental, *as it allows the X–O–X bond angles to be achieved.* The need for a polarization function to reproduce a bent arrangement around the X–O–X moiety has already been observed for the disiloxanes and silicates [32,33], and resembles the requirement of such a function on the nitrogen atom in order to describe the pyramidal geometry of amines [34,35].

When considering a polarization function on the oxygen atoms, a significant improvement of the Re–O–Re bond angle description was observed by splitting the transition metal basis set. The use of the minimal valence shell at the Re atom greatly overestimates the bridging bond angle ($\sim 13^\circ$). In contrast, when a double-zeta splitting scheme is considered at the transition metal atom, a good molecular description

of the Re_2O_7 heptoxide, in particular of the bridging bond angle, with a deviation of just 1° at the HF level.

With this basis set combination, the further splitting of the oxygen basis set did not yield any structural or vibrational frequency improvement for the systems under study while a significant increase of the average CPU time *per* optimization cycle was observed. The same conclusion was reached when a diffuse function was considered at the terminal and/or bridge oxygen atoms.

In short, from the above-mentioned results we can conclude that the use of both a polarization function at the oxygen atoms and the splitting of the transition metal valence shell are the fundamental requirements for a reasonable description of the Re_2O_7 molecular structure in the gas phase.

3.2. Energies and molecular structures

Fig. 1 shows the several configurations tested and fully optimized for each considered heptoxide. This includes all the possible configurations for a $\text{X}_2\text{O}_7^{n-}$ ($n = 4, 2, 0$) system with equivalent X– O_t bonds and nearly regular tetrahedral angles around the X atoms. Unusually distorted geometries, such as the one reported for $\text{Ge}_2\text{O}_7^{6-}$ anion in the $\text{Er}_2\text{Ge}_2\text{O}_7$ crystal [6] have not been tested.

Table 1 shows the calculated energy differences between the several optimized geometries and the minimum energy configuration, at both HF and DFT (B3LYP) levels, for the nine transition metal heptoxides herein considered. The number of imaginary frequencies (λ) obtained at the HF level for each optimized structure is also included, showing that only one energy minimum was found for each heptoxide.

There is an overall agreement between the HF and DFT results in what concerns the conformational preferences of the several heptoxides. Most of the heptoxides display a single minimum in a staggered conformation, either D_{3d} or C_2 . However, the inclusion of the electron correlation effects leads to an evident narrowing of the energy differences between the stationary points found for each system.

The heptoxides of the VB group (V, Nb and Ta) constitute a special series, as all the tested geometries converged to one of the linear structures (D_{3d} or D_{3h})

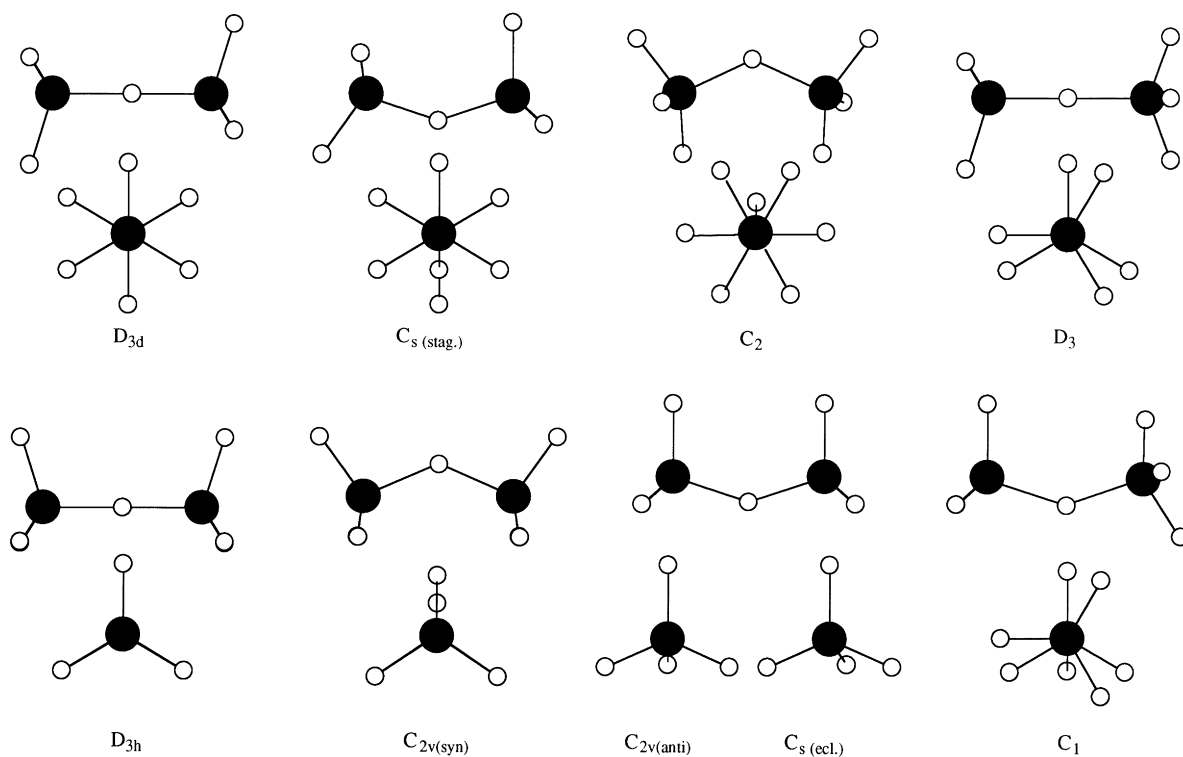


Fig. 1. Representation of the molecular geometries considered for the transition metal heptoxides studied.

at both theory levels. Vibrational frequency calculations confirmed the D_{3d} configuration to be the energy minimum, as the higher energy D_{3h} symmetry structures present an imaginary vibrational frequency for the torsional mode. This is in accordance with our previous result on $V_2O_7^{4-}$ [18].

In contrast, for the heptoxides of the VIB group (Cr, Mo, W) several tested geometries of Fig. 1 were successfully optimized. The energy differences between the bent-staggered C_2 and C_s structures are very small at the DFT (B3LYP) level and negligible at the HF level, in particular for the $Mo_2O_7^{2-}$ and $W_2O_7^{2-}$ heptoxides. The vibrational frequency calculations performed suggest that all three heptoxides present a C_2 configuration as the only energy minimum. However, some caution should be taken as the lowest wavenumbers for C_2 and C_s structures of $Mo_2O_7^{2-}$ and $W_2O_7^{2-}$ are quite low ($<10\text{ cm}^{-1}$). This fact, together with the extremely low energy difference between the two geometries, does not allow definite conclusions about the real energy-minimum geometry.

In what concerns the VIIB group a relatively scattered behaviour is noted. For Mn_2O_7 heptoxide only the minimum $C_{2v(syn)}$ and the linear (D_{3d} and D_{3h}) structures were successfully optimized at both levels. All the other geometries tested either failed to converge in the SCF procedure or fell to one of the previous during geometry optimization. In addition, the energy difference between the minimum and the linear configurations is quite large. This result suggests the uniqueness of the $C_{2v(syn)}$ structure, what is in agreement with previous ab initio calculations at the 3-21G level [36]. In addition, both Simon et al. [37] and Dronskowski et al. [38] have found the $C_{2v(syn)}$ geometry for this heptoxide in the crystal by X-ray.

Tc_2O_7 displays the most relevant difference between the HF and DFT results. In fact, while at the HF level there is a slight preference for the C_2 geometry, in similarity to the heavier Re_2O_7 analogue (see Table 1), the DFT calculations yield C_2 and $C_{2v(syn)}$ structures with nearly identical energy. As stated earlier, a recent gas-phase study seems to

Table 1

Calculated energy differences ($\Delta E/\text{kJ mol}^{-1}$) between the several optimized geometries, relative to the energy minimum, for each transition metal heptoxide studied. The number of calculated imaginary vibrational frequencies, λ (0, 1 and 2 stand for minimum, first- and second-order saddle points, respectively), are also included

Structure	$\text{V}_2\text{O}_7^{4-}$			$\text{Cr}_2\text{O}_7^{2-}$			Mn_2O_7		
	HF	λ	DFT ^a	HF	λ	DFT ^a	HF	λ	DFT ^a
C_2	–	–	–	0.00	0	0.00	–	–	–
C_s	–	–	–	0.45	1	0.50	–	–	–
$\text{C}_{2v(\text{syn})}$	–	–	–	0.91	1	0.30	0.00	0	0.00
$\text{C}_{2v(\text{anti})}$	–	–	–	3.79	2	2.69	–	–	–
D_{3d}	0.00	0	0.00	8.99	1	6.62	38.47	2	25.98
D_{3h}	0.84	1	0.47	9.09	2	6.56	37.22	2	24.81
	$\text{Nb}_2\text{O}_7^{4-}$			$\text{Mo}_2\text{O}_7^{2-}$			Tc_2O_7		
C_2	–	–	–	0.00	0	0.00	0.00	0	0.04
C_s	–	–	–	0.03	1	0.15	0.64	1	0.58
$\text{C}_{2v(\text{syn})}$	–	–	–	0.87	1	0.53	0.17	0	0.00
$\text{C}_{2v(\text{anti})}$	–	–	–	1.30	2	0.83	3.02	2	2.39
D_{3d}	0.00	0	0.00	1.81	1	1.07	11.01	1	7.78
D_{3h}	0.75	1	0.64	2.15	2	1.28	10.63	2	7.52
	$\text{Ta}_2\text{O}_7^{4-}$			$\text{W}_2\text{O}_7^{2-}$			Re_2O_7		
C_2	–	–	–	0.00	0	0.00	0.00	0	0.00
C_s	–	–	–	0.00	1	0.09	0.13	1	0.38
$\text{C}_{2v(\text{syn})}$	–	–	–	0.42	1	0.12	0.28	1	0.45
$\text{C}_{2v(\text{anti})}$	–	–	–	0.42	2	^b	1.19	2	1.13
D_{3d}	0.00	0	0.00	0.12	1	0.26	3.89	1	2.90
D_{3h}	0.63	1	0.40	0.43	2	0.40	3.77	2	2.77

^a DFT = B3LYP.

^b Converged to $\text{C}_{2v(\text{syn})}$ symmetry during geometry optimization.

support the similarity between the geometries of the Tc_2O_7 and Re_2O_7 heptoxides [3].

Re_2O_7 follows the general behaviour of the previous group at both levels. The lowest energy structure is the C_2 geometry, while C_s and $\text{C}_{2v(\text{syn})}$ structures are the nearest saddle points (energy differences below 1 kJ mol^{-1}).

The calculated structural parameters obtained for the minimum energy configuration of the several transition metal heptoxides, at both HF and DFT levels, are presented in Table 2, in comparison with experimental data available. It is worth to note that all the experimental data, except those of Re_2O_7 , refer to solid samples.

The overall agreement between the calculated values and the corresponding literature experimental

results can be considered excellent. In fact, the average difference between the calculated and the experimental X–O bond lengths and O–X–O bond angles are less than 2 pm and 2° , respectively. The largest differences are observed for the Mo–O bond lengths and for the $\text{O}_b\text{–V–O}_t$ bond angle, which are overestimated by 5 pm and 6° , respectively.

The agreement between the experimental and the calculated bridging bond angles X– O_b –X, is also very good. The largest difference is observed for the Mn– O_b –Mn bond angle, which is overestimated at both levels by 4° . In the case of the $\text{Mo}_2\text{O}_7^{2-}$ heptoxide, a similar difference of 4° in the Mo– O_b –Mo structural parameter at the HF level is corrected by the inclusion of the electron correlation effects.

In what concerns the $\text{V}_2\text{O}_7^{4-}$ and $\text{Cr}_2\text{O}_7^{2-}$ anions, the calculated values of 180° and 138° (137° at the HF level) for the V– O_b –V and Cr– O_b –Cr bond angles, respectively, are both within the range of the experimental data [6].

3.3. Vibrational wavenumbers

Tables 3, 4 and 5 present the calculated vibrational wavenumbers for the minimum energy configurations of the several heptoxides, presenting a D_{3d} , C_2 or $\text{C}_{2v(\text{syn})}$ symmetry, respectively.

The experimental information on the vibrational spectra of these heptoxides is quite scarce. In fact, a relatively complete vibrational assignment was only found for the $\text{Cr}_2\text{O}_7^{2-}$, Mn_2O_7 and Re_2O_7 heptoxides. The overall agreement between the calculated vibrational wavenumbers and the experimental values available is reasonable. Even in the case of the dichromate anion, for which most of the experimental assignments refer to the solid state, the ordering of the different vibrational modes is perfectly described by the calculations herein reported.

A question that raised some attention recently [44] concerns the relative ordering of the symmetric and antisymmetric $-\text{XO}_3$ stretching modes ($\nu_s\text{XO}_3$ and $\nu_{\text{as}}\text{XO}_3$, respectively) on this kind of systems. The results on Tables 3, 4 and 5 show that only in the cases of the light $\text{Cr}_2\text{O}_7^{2-}$ and Mn_2O_7 heptoxides the antisymmetric stretching modes occur at a higher frequency than the symmetric ones. In all the remaining systems each $\nu_s\text{XO}_3$ mode is above the corresponding $\nu_{\text{as}}\text{XO}_3$. This distinction between the

Table 2

Optimized parameters for the minimum of each transition metal heptoxide studied. Experimental results are included, whenever existante

Heptoxide		X–O _b pm ^a	X–O _t pm ^a	O _b –X–O _t deg. ^a	O _t –X–O _t deg. ^a	X–O _b –X deg. ^a	Symmetry
V ₂ O ₇ ⁴⁻	Calc. HF	181	164	110	109	180	D _{3d}
	Calc. DFT ^b	181	168	111	108	180	D _{3d}
	Exp. ^c	180	167	105	113	117–180	
Nb ₂ O ₇ ⁴⁻	Calc. HF	199	180	110	109	180	D _{3d}
	Calc. DFT ^b	203	185	111	108	180	D _{3d}
Ta ₂ O ₇ ⁴⁻	Calc. HF	196	180	110	109	180	D _{3d}
	Calc. DFT ^b	200	184	111	108	180	D _{3d}
Cr ₂ O ₇ ²⁻	Calc. HF	174	155	106–110	111	137	C ₂
	Calc. DFT ^b	178	162	106–111	110	138	C ₂
	Exp. ^d	178	161	109	110	121–145	C ₂
Mo ₂ O ₇ ²⁻	Calc. HF	189	171	107–110	110	150	C ₂
	Calc. DFT ^b	193	177	108–110	109	154	C ₂
	Exp. ^e	188	172	110	109	154	C ₂
W ₂ O ₇ ²⁻	Calc. HF	188	172	108–110	110	165	C ₂
	Calc. DFT ^b	191	177	109–111	109	166	C ₂
Mn ₂ O ₇	Calc. HF	174	150	102–106	114	125	C _{2v(syn)}
	Calc. DFT ^b	175	156	105–108	111–112	125	C _{2v(syn)}
	Exp. ^f	176	158	108	111	121	C _{2v(syn)}
C ₂	Calc. HF	186	165	106–107	112	135	
	Calc. DFT ^b	189	171	107–109	109–111	135	C _{2v(syn)}
	Exp. ^g	184	170			< 180	C ₂
Re ₂ O ₇	Calc. HF	185	166	107–108	111	145	C ₂
	Calc. DFT ^b	188	171	108–110	110	146	C ₂
	Exp. ^h	189	171	110		144	C ₂

^a O_b and O_t stand for bridge and terminal oxygens, respectively.^b DFT = B3LYP.^c See footnote of Table 8 of Ref. [18] and Refs. [6,39].^d Refs. [6,40].^e Ref. [41].^f Refs. [37,38].^g Ref. [3].^h Ref. [2].

lighter (with $\nu_s \text{XO}_3 < \nu_{as} \text{XO}_3$) and the heavier (with $\nu_s \text{XO}_3 > \nu_{as} \text{XO}_3$) transition metal compounds does not hold in the case of the linear V₂O₇⁴⁻ ion, stressing the importance of the molecular geometry in the ordering of the vibrational modes.

In the region of the low wavenumber modes, both the torsion and the skeletal X–O_b–X bend deserve particular attention. The torsional wavenumbers are generally quite low, and should be considered with caution. All the lowest energy-structures present real numbers for the torsional modes, but the barriers to internal rotation of the –XO₃ groups are clearly soft.

Mo₂O₇²⁻ and W₂O₇²⁻ heptoxides present the lowest $\delta \text{X–O}_b\text{–X}$ wavenumbers for this series of oxyanions, in agreement with the flat potential well expected for a

nearly linear structure. The highest wavenumber is found for Mn₂O₇, which also presents the smallest X–O_b–X angle. An interesting behaviour is observed for the $\delta \text{X–O}_b\text{–X}$ mode in the case of the linear heptoxides (VB group). As it can be seen on Table 3, the wavenumber of this mode increases along the group (V, Nb, Ta). As the metal atom mass increases in the same direction, the increase of the $\delta \text{X–O}_b\text{–X}$ wavenumber can only be explained by an increase of the corresponding force constant from V₂O₇⁴⁻ to Ta₂O₇⁴⁻.

4. Discussion

Fig. 2 shows a representation of the DFT calculated

Table 3
HF calculated vibrational wavenumbers^a (cm⁻¹) and corresponding assignments for the linear heptoxides

Symmetry	V ₂ O ₇ ⁴⁻ Calc.	Nb ₂ O ₇ ⁴⁻ Calc.	Ta ₂ O ₇ ⁴⁻ Calc.	Approximate Description ^b
a _{1g}	959	877	882	$\nu_s \text{XO}_3$
	392	316	290	$\delta_s \text{XO}_3$
	190	156	140	$\nu_s \text{X-O}_b$
e _g	760	788	775	$\nu_{as} \text{XO}_3$
	328	270	272	$\delta_{as} \text{XO}_3$
	213	174	170	$\rho_s \text{XO}_3$
a _{1u}	13	12	10	$\tau_s \text{OX-XO}$
a _{2u}	948	877	891	$\nu_s \text{XO}_3$
	668	647	681	$\nu_{as} \text{X-O}_b$
	312	272	266	$\delta_s \text{XO}_3$
e _u	814	793	779	$\nu_{as} \text{XO}_3$
	346	284	285	$\delta_{as} \text{XO}_3$
	294	256	266	$\rho_{as} \text{XO}_3$
	57	65	70	$\delta \text{X-O}_b\text{-X}$

^a Calculated wavenumbers were scaled by a factor of 0.9.

^b ν = stretching; δ = bending; ρ = rocking; τ = torsion; s = symmetric; as = antisymmetric; b = bridge.

Table 4
HF calculated vibrational wavenumbers^a(cm⁻¹) and corresponding assignments for the staggered bent (C₂) heptoxides

Symmetry	Cr ₂ O ₇ ²⁻		Mo ₂ O ₇ ²⁻	W ₂ O ₇ ²⁻	Re ₂ O ₇		Approximate description ^a	
	Calc.	Exp. ^b	Calc.	Calc.	Calc.	Exp. ^c		
A	1051	901	1001	1014	1109	1008	$\nu_s \text{XO}_3$	
	1090	960	966	946	1067	971	$\nu_{as} \text{XO}_3$	
	1074	922	956	940	1064	971	$\nu_{as} \text{XO}_3$	
	555	555	418	344	430	480	$\nu_s \text{X-O}_b$	
	428	386	328	320	344	342	$\delta_{as} \text{XO}_3$	
	409		320	342	338	342	$\delta_{as} \text{XO}_3$	
	243	137	190	178	311	305?	$\rho_s \text{XO}_3$	
	397	362	311	302	181		$\delta_s \text{XO}_3$	
	239		185	172	178	174	$\rho_{as} \text{XO}_3$	
	69	89	16	24	46	61	$\delta \text{X-O}_b\text{-X}$	
	23		15	10	12		$\tau_s \text{OX-O}_b\text{X}$	
	B	1034	884	995	1020	1107	1050	$\nu_s \text{XO}_3$
		1090	938	967	946	1069	971	$\nu_{as} \text{XO}_3$
1070		884	955	940	1062	971	$\nu_{as} \text{XO}_3$	
808		758	788	833	858	868	$\nu_{as} \text{X-O}_b$	
415		372	323	320	343	342	$\delta_{as} \text{XO}_3$	
414		334	320	318	338	342	$\delta_{as} \text{XO}_3$	
359		232	287	292	306	305?	$\rho_s \text{XO}_3$	
405		386	313	299	290	305?	$\delta_s \text{O}_3$	
238		213	182	178	177	174	$\rho_{as} \text{XO}_3$	
32			10	3	18		$\tau_{as} \text{OX-O}_b\text{X}$	

^a See footnotes of Table 3.

^b Ref. [42].

^c Ref. [3].

Table 5
Mn₂O₇ HF calculated vibrational wavenumbers^a (cm⁻¹) and corresponding assignments

Symmetry	Calc.	Exp. ^b	Approximate description ^a
A ₁	1141	960	$\nu_{as}O_3$
	973	891	ν_sXO_3
	529	555	ν_sX-O_b
	406	≈ 350	$\delta_{as}XO_3$
	382		δ_sXO_3
	226		$\rho_{as}XO_3$
A ₂	106		$\delta X-O_b-X$
	1153		$\nu_{as}XO_3$
	392		$\delta_{as}XO_3$
	233		ρ_sXO_3
B ₁	16		τ_sOX-O_bX
	1154	891	$\nu_{as}XO_3$
	400		$\delta_{as}X-O_3$
	363		ρ_sXO_3
B ₂	77		$\tau_{as}OX-O_bX$
	1131	955	$\nu_{as}XO_3$
	974	955	ν_sXO_3
	748	780	$\nu_{as}X-O_b$
	398		$\delta_{as}X-O_3$
	332		δ_sX-O_3
	216		$\rho_{as}XO_3$

^a See footnotes of Table 3.

^b Ref. [43].

energy differences (below 3 kJ mol⁻¹) between the minimum and the other stationary structures found for heptoxides studied, sorted by increasing value of the X–O_b–X angle. This Fig. allows the assessment of some general trends in this set of heptoxides.

For instance, it can be seen that there is a smooth decrease of the energy difference between C_S and C₂ forms from Tc to W heptoxides, following the increase of the X–O_b–X angle. As the difference between the two structures arises from the rotation of the X–O_b–X plane relative to the X–X–O_t plane (see Fig. 1), their energy difference naturally tends to vanish with increasing linearity of the X–O_b–X fragment. The same trend is observed for the energy difference between the C_{2v(anti)} form and the less hindered C_{2v(syn)} form.

The preference of Mn₂O₇ for a C_{2v(syn)} eclipsed structure is particularly meaningful as it shows that the steric hindrance is not the only factor that rules the energy difference between the staggered and eclipsed forms. A possible explanation for this conformational preference lies on the repulsion between the X–O_t bonds and the electron lone pairs of the bridging oxygen atom in a nearly sp³ hybridization. In fact, it has been claimed [38] that the decrease of the bridging bond angle (increase of the sp³ character) should be correlated with an eclipsed configuration.

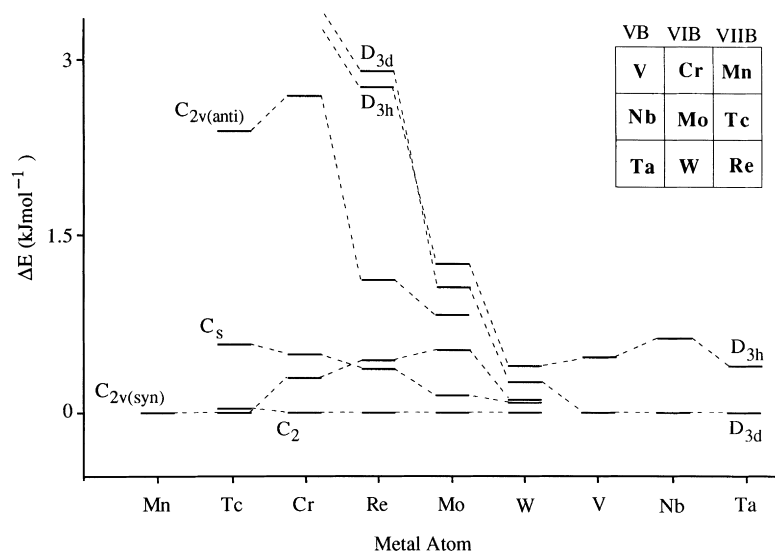


Fig. 2. Energy differences between the minimum and the low-lying stationary points for the transition metal heptoxides studied (only the differences below 3 kJ mol⁻¹ are shown).

The most clear trend observed in Fig. 2 is the relative stabilization of the linear D_{3h} and D_{3d} forms (or, in other words, the decrease of the barrier to linearization of the $X-O_b-X$ fragment) on going from Mn to Ta, which brings back the question on the linearity of these systems. As it can be seen from Fig. 2, the stability of the linear forms correlates with the position of the metal atom in the Periodic Table. In fact, within each period the $X-O_b-X$ angle decreases from left to right, while an increase is observed from top to bottom in the case of groups VIB and VIIB. In what concerns group VB, the three heptoxides are already linear but the above-mentioned increase of the force constant for the $\delta X-O_b-X$ mode means that the rigidity of the linear structure also increases along the group.

In this way, it can be concluded that the tendency to linearity of the $X-O_b-X$ skeleton for the heptoxides herein considered increases *backwards* each period and *downwards* each group (see Table 2). Such a regular behaviour can be explained by three main factors: (i) the total electronic charge of the heptoxides, (ii) the transition metal atom size and (iii) the π -bonding interaction between the two filled 2p orbitals of the bridging oxygen atom and the empty d orbitals of the metal atoms.

The total charge of the heptoxide can be important to explain the behaviour within each period. Assuming that the charge is mainly localized at the two $-XO_3$ fragments, the repulsion between them will be minimised in the linear structure. In this way, the increase of net charge will lead to the opening of the $X-O_b-X$ angle.

The steric hindrance between the XO_3 fragments is also associated with the size of the metal atom and can be called to understand the increasing linearity along a group. Steric effects were claimed to be enough to explain the large Si–O–Si angle in disiloxane ($H_3Si-O-SiH_3$) [32], for which no (p–d) π bonding was observed. However, in the case of the transition metal heptoxides, the explanation of the observed trends based on steric effects alone is not fully satisfactory. For instance, the effect of the metal atom size is not straightforward, as the increase of the atomic radius can be also followed by the increase of the $X-O_b$ bond length, pushing apart the two $-XO_3$ fragments. However, preliminary calculations for main group element heptoxides with the same net charge

as those of group VB, such as $P_2O_7^{4-}$, did not yield linear structures as energy minima.

Thus, the interaction between the two 2p orbitals of the bridging oxygen atom and the d orbitals of the metal atoms should play an important role in the structure of these systems. This kind of interaction was firstly proposed to justify the linearity of the $Ru_2Cl_{10}O^{4-}$ skeleton [45] and has already been considered in the case of some heptoxides [46]. As the stronger p–d interaction will occur with the best orbital overlap and with the smallest energy difference between orbitals, the effectiveness of such interaction is expected to be smaller in Si and P systems and larger in transition metal containing systems. *In what concerns the metal heptoxides, the calculated energy difference between the 2p orbitals of a O^{2-} anion and the valence d orbitals of the X^{n+} metal ions decreases backwards each period and downwards each group (i.e. parallels the increase of the $X-O_b-X$ angle). In this way, by assuming the $X-O_b-X$ angle fragment as a $X^{n+}O^{2-}X^{n+}$ association, the observed tendency to linearity in these systems can be explained by the extent of the p–d interactions alone.*

Acknowledgements

The authors acknowledge financial support from the Fundação para a Ciência e a Tecnologia (FCT), Lisboa, Portugal.

References

- [1] V.S. Vinogradov, V.V. Ugarov, N.G. Rambidi, J. Struct. Chem. 13 (1972) 661.
- [2] P. Kiprof, W.A. Herrmann, F.E. Kühn, W. Scherer, M. Kleine, M. Elison, K. Rypdal, H.V. Volden, S. Gundersen, A. Haaland, Bull. Soc. Chim. Fr. 129 (1992) 655.
- [3] I.R. Beattie, T.R. Gilson, P.J. Jones, Inorg. Chem. 35 (1996) 1301.
- [4] B. Krebs, Angew. Chem. Int. Ed. Engl. 8 (1969) 381.
- [5] B. Krebs, Z. Anorg. Allg. Chem. 380 (1971) 146.
- [6] G.M. Clark, R. Morley, Chem. Soc. Rev. 5 (1976) 269.
- [7] H.J. Becher, D. Fenske, J. Chem. Res. (1978) 167.
- [8] K. Stadnicka, J. Haber, R. Kozłowski, Acta Crystallogr. B33 (1977) 3859.
- [9] W.P. Griffith, H.I.S. Nogueira, A.J.P. White, D.J. Williams, Polyhedron 16 (1997) 1323.

- [10] G. Frenking, I. Antes, M. Böhme, S. Dapprich, A.W. Ehlers, V. Jonas, A. Neuhaus, M. Otto, R. Stegmann, A. Veldkamp, S.F. Vyboishchikov, *Rev. Comp. Chem.* 8 (1996) 63.
- [11] T.V. Russo, R.L. Martin, P.J. Hay, *J. Phys. Chem.* 99 (1995) 17085.
- [12] G. Frenking, U. Pidun, *J. Chem. Soc., Dalton Trans.* (1997) 1653.
- [13] G. Orlova, S. Scheiner, *J. Phys. Chem. A* 102 (1998) 4813.
- [14] M. Kaupp, V.G. Malkin, O.L. Malkina, D.R. Salahub, *J. Am. Chem. Soc.* 117 (1995) 1851.
- [15] T. Wagener, G. Frenking, *Inorg. Chem.* 37 (1998) 1805.
- [16] F.A. Cotton, X. Feng, *J. Am. Chem. Soc.* 119 (1997) 7514.
- [17] A. Ignaczak, J.A.N.F. Gomes, *Chem. Phys. Lett.* 257 (1996) 609.
- [18] P.J.A. Ribeiro-Claro, A.M. Amado, J.J.C. Teixeira-Dias, *J. Comp. Chem.* 17 (1996) 1196.
- [19] Gaussian 94, Revision E.3, M.J. Frisch, G.W. Trucks, H.B. Schlegel, P.M.W. Gill, B.G. Johnson, M.A. Robb, J.R. Cheeseman, T. Keith, G.A. Petersson, J.A. Montgomery, K. Raghavachari, M.A. Al-Laham, V.G. Zakrzewski, J.V. Ortiz, J.B. Foresman, J. Cioslowski, B.B. Stefanov, A. Nanayakkara, M. Challacombe, C.Y. Peng, P.Y. Ayala, W. Chen, M.W. Wong, J.L. Andres, E.S. Replogle, R. Gomperts, R.L. Martin, D.J. Fox, J.S. Binkley, D.J. Defrees, J. Baker, J.P. Stewart, M. Head-Gordon, C. Gonzalez, J.A. Pople, Gaussian, Inc., Pittsburgh, PA, 1995.
- [20] W.J. Stevens, H. Basch, M. Krauss, *J. Chem. Phys.* 81 (1984) 6026.
- [21] P.J. Hay, W.R. Wadt, *J. Chem. Phys.* 82 (1985) 299.
- [22] W.J. Heyre, L. Radom, R.v.R. Schleyer, J.A. Pople, *Ab initio molecular orbital theory*, Wiley, New York, 1986, p. 82.
- [23] T. Clark, J. Chandrasekhar, G.W. Spitznagel, R.v.R. Schleyer, *J. Comp. Chem.* 4 (1983) 294.
- [24] P.J. Hay, W.R. Wadt, *J. Chem. Phys.* 82 (1985) 270.
- [25] V. Jonas, G. Frenking, M.T. Reetz, *J. Comp. Chem.* 13 (1992) 919.
- [26] A. Veldkamp, G. Frenking, *J. Comp. Chem.* 13 (1992) 1184.
- [27] A. Veldkamp, G. Frenking, *Chem. Ber.* 126 (1993) 1325.
- [28] A. Ignaczak, J.A.N.F. Gomes, *J. Electroanal. Chem.* 420 (1997) 209.
- [29] F.A. Cotton, X. Feng, *J. Am. Chem. Soc.* 120 (1998) 3387.
- [30] C. Lee, W. Yang, R.G. Parr, *Phys. Rev. B* 37 (1988) 785.
- [31] A. Becke, *J. Chem. Phys.* 98 (1993) 5648.
- [32] S. Grigoras, T.H. Lane, *J. Comp. Chem.* 8 (1987) 84.
- [33] C.W. Earley, *J. Comp. Chem.* 14 (1993) 216.
- [34] L.A.E. Batista de Carvalho, A.M.A. da Costa, J.J.C. Teixeira-Dias, *J. Molec. Struct. (Theochem)* 205 (1990) 327.
- [35] L.A.E. Batista de Carvalho, J.J.C. Teixeira-Dias, *J. Molec. Struct. (Theochem)* 282 (1993) 199.
- [36] P.J.A. Ribeiro-Claro, 2nd European Conference on Computational Chemistry, Lisbon, 1997.
- [37] A. Simon, R. Dronskowski, B. Krebs, B. Hettich, *Angew. Chem. Int. Ed. Engl.* 26 (1987) 139.
- [38] R. Dronskowski, B. Krebs, A. Simon, G. Müller, B. Hettich, *Z. Anorg. Allg. Chem.* 558 (1988) 7.
- [39] R. Gopal, C. Calvo, *Acta Crystallogr. B* 30 (1974) 2491.
- [40] J.K. Brandon, I.D. Brown, *Can. J. Chem.* 46 (1968) 933.
- [41] V.W. Day, M.F. Fredrich, W.G. Klemperer, W. Shum, *J. Am. Chem. Soc.* 98 (1977) 6146.
- [42] M.H. Abbas, D. Davidson, *Spectrochim. Acta* 50A (1994) 1153.
- [43] W. Levason, J.S. Ogden, J.W. Turff, *J. Chem. Soc. Dalton Trans.* (1983) 2699.
- [44] J. Cejka, private communication.
- [45] J.D. Dunitz, L.E. Orgel, *J. Chem. Soc.* (1953) 2594.
- [46] D.W. Cruickshank, *J. Chem. Soc.* (1961) 5486.